Mechanical Systems and Signal Processing 224 (2025) 111942

Contents lists available at ScienceDirect

Mechanical Systems and Signal Processing

journal homepage: www.elsevier.com/locate/ymssp

Actuator saturation during active vibration control of milling

Muhammet Ozsoy [a,b,*], Neil D. Sims [a], Erdem Ozturk [c]

[a] Department of Mechanical Engineering, The University of Sheffield, S1 3JD, Sheffield, UK
[b] Department of Mechanical Engineering, Eskisehir Technical University, 26555, Eskisehir, Turkey
[c] Advanced Manufacturing Research Center, The University of Sheffield, Wallis Way, Rotherham, S1 3JD, Sheffield, UK

ARTICLE INFO

Communicated by X. Si

Keywords:
Robotic assisted milling
Active chatter control
Saturation model
Chatter stability
Inertial actuator

ABSTRACT

Machining chatter is a common problem in the manufacturing industry that can lead to reduced productivity, poor surface quality, and accelerated tool wear. Various methods have been proposed to suppress chatter, including passive, active, and hybrid techniques. Active control methods, in particular, have gained increasing attention due to their potential for achieving higher suppression effectiveness and adaptability to different machining conditions. However, one of the main challenges of active control is the occurrence of actuator saturation, which happens when the actuator reaches its maximum output and cannot provide any further control action. This can lead to instability and deterioration of suppression performance. Despite its significance, the issue of actuator saturation in machining chatter suppression has not received much attention in the literature. Therefore, this paper aims to fill this gap by providing a detailed investigation of the effects of actuator saturation on the performance of active control methods for chatter suppression. The paper presents a comprehensive review of existing literature on machining chatter suppression methods, with a specific focus on active control techniques and their associated problems, such as saturation. An experimental scenario is presented that illustrates the problem of actuator saturation in the context of robotically assisted milling. The paper then proposes a novel actuator saturation model in the frequency domain that can significantly inform the selection of cutting parameters, potentially enhancing material removal rates and operational productivity. By addressing this research problem, this paper aims to make a significant contribution to the field of machining chatter suppression and stimulate further research in this direction.

1. Introduction

Regenerative chatter remains a significant impediment in machining processes, leading to detrimental effects such as self-excited vibrations, elevated cutting forces, compromised surface quality, and accelerated tool wear [1]. Particularly impacting on thin-walled and flexible structures due to their low dynamic stiffness, chatter necessitates robust mitigation strategies.

In pursuit of establishing precise mathematical models, extensive studies have been conducted on the chatter mechanism [2,3]. Altintas and Budak [4–7] expanded the theory of regenerative chatter by considering both the tool and workpiece as multi-degree-of-freedom structures. Their approach involved the development of a stability model by analysing the time-periodic equation of motion using a Fourier series expansion. This method accurately predicts the boundaries of chatter; meanwhile Insperger and Stepan [8–10] introduced the semi-discretisation method, to efficiently account for the time period coefficients.

* Corresponding author at: Department of Mechanical Engineering, Eskisehir Technical University, 26555, Eskisehir, Turkey.
E-mail address: muhammet.ozsoy@eskisehir.edu.tr (M. Ozsoy).

https://doi.org/10.1016/j.ymssp.2024.111942
Received 31 May 2024; Received in revised form 3 September 2024; Accepted 9 September 2024
Available online 11 October 2024

Additional damping and structural alterations have proven effective in enhancing chatter stability [11,12], or newly designed cutting tools to improve vibration suppression performance [13]. However, passive methods like tuned mass dampers (TMDs) require manual intervention and lack adaptability to changing system configurations. This issue can be avoided by implementing a semi-active chatter reduction method [14] or an active damping system [15] and also higher performance can be obtained via active control methods.

Early research efforts in active chatter control focused on improving boring operations. Klein and Nachtigal [16,17] proposed an active control scheme utilising an electrohydraulic servo system to enhance boring bar performance. Experimental findings demonstrated a significant improvement in the critical limiting depth of cut. However, they noted that the performance of active vibration control depended on understanding the principal modes and cutting force angle. Similarly, Glaser and Nachtigal [18] investigated a special boring bar with two hydraulic chambers for actuation. However, control system limitations hindered optimal chatter control performance.

Active regenerative chatter control techniques have also been applied in milling operations. For instance, Munoa et al. [19] developed a biaxial active actuator, comparing one and two-axis actuators in experiments. Two-axis actuators demonstrated enhanced machining stability, resulting in more accurate operations. Monnin et al. [20,21] introduced an active control system integrated into a spindle unit, utilising four piezoelectric stack actuators with equal spacing. Various control methods, including adaptive control [22], model-predictive control [23], H_∞ [24], and a robust control [25,26], were investigated for integrating piezoelectric stack actuators into spindle units. Zhang and Sims [27] explored a piezoelectric patch actuator for active damping in milling operations, reporting an increase in the critical depth of cut through positive position feedback control strategy. Using the piezoelectric patch actuator can pose challenges regarding mounting. Additionally, in numerous tests, controller performance was degraded by actuator saturation.

Alternative methods have been proposed to enhance chatter stability. Huyanan and Sims [28] presented three control methods, the skyhook controller (DVF), the virtual passive absorber (VPA), and the virtual active tuned mass damper (VATMD). A proof-mass actuator was attached to the workpiece to reduce the vibrations. The cutting tests were presented using the virtual passive absorber method tuned by Sims method [29]. Due to the material removal effect, the dynamic properties of the structure were changed, which caused stability degradation. To overcome this problem, automatically tuned actuators were examined. Beudaert et al. [30] developed a portable inertial actuator capable of automatic controller parameter tuning for flexible structures, demonstrating improved dynamic properties in experimental and industrial settings. Also, Zaeh et al. [31] introduced an automatically tuned inertial actuator for machining vibration suppression, employing direct velocity feedback (DVF) and H_∞ control methods to enhance stability. Moreover, Kleinwort et al. [32] proposed a particle swarm optimisation-based automatic tuning method for active vibration control, comparing its performance with existing control methods in cutting tests. Validation of controller performance were carried out for DVF, H_∞ and a novel adaptive FxLMS control [33]. Significantly improved chatter stability was achieved by implementing the active control methods.

Additionally, alternative active control solutions such as the new machine tool feed drive system [34,35] and designing active workpiece holders [36] have been explored to mitigate chatter. Active magnetic bearing (AMB) systems [37], despite promising advantages such as increased system stiffness, face technical challenges including low specific load, bandwidth limitations, and spindle dynamics complexity, which must be addressed for future applications.

Active damping systems have gained traction in recent years [19,38], utilising inertial actuators and control strategies such as direct velocity feedback (DVF) [39,40]. Model-based approaches such as Linear Quadratic Regulator (LQR) and H_∞ control exhibit promise, yet necessitate prior knowledge of structural dynamics for effective parameter tuning [31,41]. The μ synthesis method offers advantages in stability and robustness, particularly in the face of uncertainties [42,43].

Recently, Ozsoy et al. [44] proposed a virtual inerter based dynamic vibration absorber (IDVA) by utilising an inertial actuator, building upon the passive chatter suppression method developed by Dogan et al. [45]. The numerical analysis revealed that an IDVA could enhance absolute chatter stability by over 20% compared to the effectiveness of a TMD. However, this improvement was constrained by the maximum actuator force utilised in the experimental setup. Subsequently, the numerical findings were validated through cutting trials [46]. They [47] also analysed the uncertainty and robustness of IDVA considering various layouts for the active control systems. The potential benefits and limitations of IDVAs, considering actuator saturation and parameter uncertainty, were demonstrated.

More broadly, robotic machining and robotic-assisted machining has earned attention, due to their potential to offer more versatility and to increase productivity [48]. Robotic-assisted machining, as explored by [49], demonstrates promise in improving form accuracy by utilising robotically-supported workpieces. This is particularly relevant when the workpiece being machined is flexible or difficult to clamp using traditional fixture designs.

Ozsoy et al. [50] proposed a novel mobile active vibration control method employing a robotic arm specifically adapted for milling operations. Later work [51] extended this to explore the experimental performance of a basic prototype from a dynamics perspective. By combining automation capabilities with vibration control, the approach aimed to overcome the challenges faced by active vibration control methods in practical production environments. They defined a simplified dynamic scenario, and introduced time-domain and frequency-domain models of the system for numerical study. Several control systems were designed and their efficiency in chatter stability prediction was evaluated through simulations validated by experimental frequency response function (FRF) tests. However, this previous work did not demonstrate the performance of the approach in a machining environment.

Based upon this literature, it is clear that active vibration control offers the potential to greatly improve machining productivity through the reduction of regenerative chatter. However, a key obstacle is the onset of actuator saturation effects, which have been shown to exist for a wide range of control strategies and implementation scenarios. Meanwhile, the practical implementation of

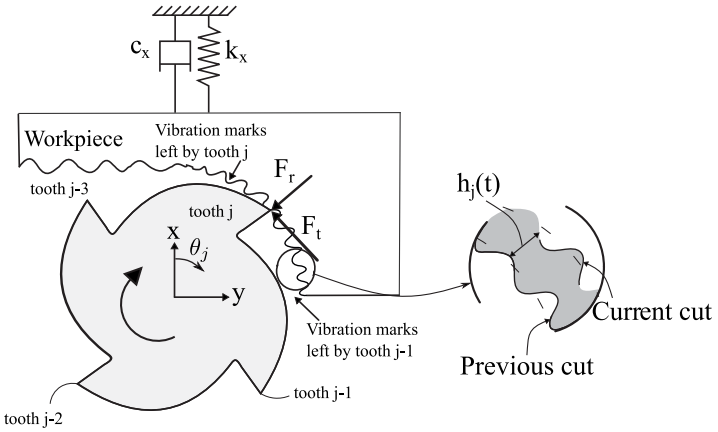

Fig. 1. Self-excited vibrations in milling.

active vibration control could be eased by combining the method with robotic and automation approaches, but this approach has not yet been tested in a machining environment.

The present contribution aims to tackle these two shortfalls. First, machining experiments are presented to verify the robotic-assisted concept in real cutting conditions. These experiments also serve to illustrate the existence of actuator saturation issues when considering the complex forced vibrations that occur during milling. Next, a novel actuator saturation model is developed to predict the interdependency between saturation effects and machining process parameters. Experimental validation demonstrates the efficacy of the saturation model in a machining context. The effect of different machining parameters and active vibration control strategies are then discussed, before drawing conclusions.

2. Background theory

To begin, it is helpful to briefly summarise regenerative chatter mechanisms and how such chatter is mitigated by active vibration control. Extensive and accurate models exist elsewhere in the literature [52,53], so this section provides only a simplified formulation.

Consider the rigid cutting tool and flexible workpiece, as illustrated in Fig. 1; here (to simplify and maintain consistency with subsequent analyses) a single coordinate x is employed. The interaction involves the rigid cutting tool inducing waviness on the flexible workpiece's surface with each cut. The phase relationship between successive waviness imprints results in variations in the instantaneous chip thickness, denoted as $h(t)$. These variations lead to instability in the cutting process, triggering exponential growth in vibrations and cutting forces.

Considering the cutting force's proportionality to the removal chip area, and simplifying the time-periodic coefficients by using the first term of a Fourier series expansion [5], the predicted stability limit in a single degree-of-freedom (SDOF) system becomes:

$$a_{cr} = \frac{-1}{\left(\frac{N_t}{2\pi}\right) b_{xx} K_c \Re\mathfrak{e}(G(j\omega_c))}. \tag{1}$$

Here, a_{cr} is the critical limiting depth of cut above which chatter occurs. Meanwhile, K_c is cutting stiffness, N_t is the number of flutes, and b_{xx} is a directional coefficient which is related to the cutting conditions and arises from the time-averaging that is introduced by the Fourier series expansion and truncation [5].

Tobias and Fishwick [2] explained the relationship between the critical limiting depth of cut and the time delay inherent in the machining process. This relationship gave rise to stability pockets, known as the stability lobe diagram (SLD). The diagram illustrates the stability boundary as a function of spindle speed and axial depth of cut. Additionally, Merritt [54] represented the chatter theory as a feedback loop system, neglecting the process damping phenomena introduced by Tobias at lower spindle speeds, and achieved stability using the Nyquist stability criterion.

From the perspective of active vibration control, the key term in (1) is $\Re\mathfrak{e}(G(j\omega_c))$. Here, ω_c is the chatter frequency, and G is the frequency response function (FRF) of the flexible structure. Therefore, chatter stability is directly related to the negative real component of the FRF. Many active vibration control approaches can directly modify this value [55], by drawing upon classical and optimal control strategies such as Direct Velocity Feedback, Linear Quadratic Regulator, and H_∞ control. Alternatively, bespoke mechanisms of feedback control can be employed, such as delayed feedback [2,54] that accounts for the special nature of regenerative chatter as a time-delayed differential equation.

3. Robotic assisted milling: experimental proof of concept

This section extends earlier work [51] by experimentally demonstrating how active vibration control could be applied as part of a robotic assisted milling operation, and to illustrate the impact of actuator saturation effects.

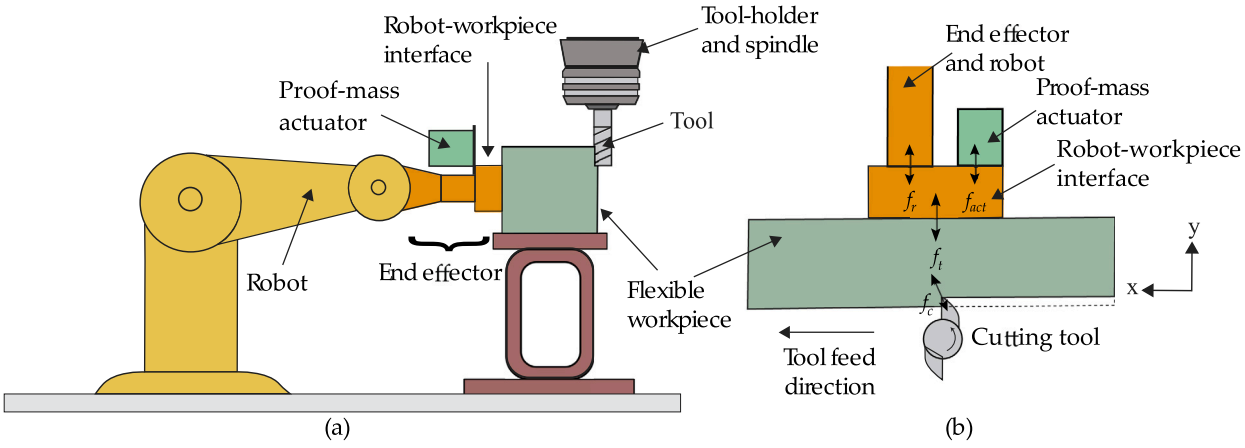

Fig. 2. Conceptual illustration of robotic assisted vibration control during milling. (a) side view; (b) top view, showing the cutting force f_c, total support force f_t, total proof-mass actuator force f_{act} and robot support force f_r.

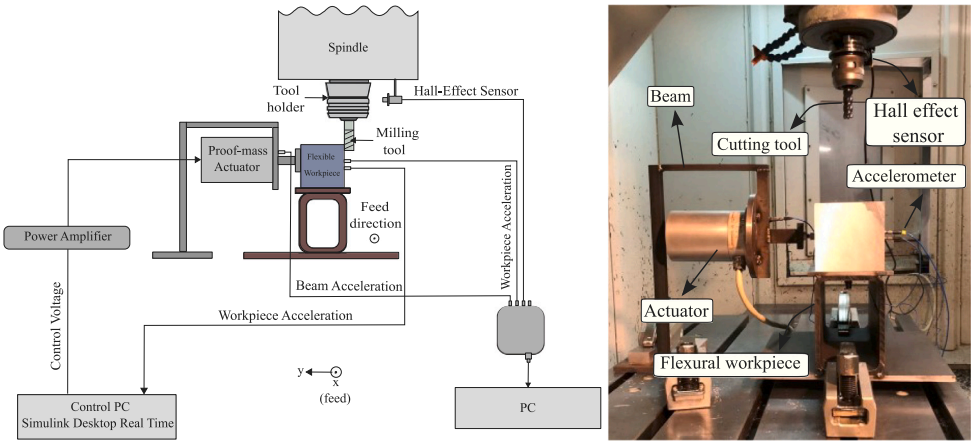

Fig. 3. Experimental setup for the milling tests.

3.1. Experimental configuration and method

The ultimate application of robotic assisted milling with active vibration control is illustrated schematically in Fig. 2. Employing a six-axis industrial robot, an end effector is positioned against the machining workpiece, which remains secured through conventional fixturing techniques. The articulated robot is strategically manoeuvred to establish a beneficial contact pressure between the end effector and the workpiece. In contrast to previous approaches [49] the primary function of the end effector is to apply dynamic forces to the workpiece through a proof-mass (or inertial) actuator. This intentional imposition of forces aims to enhance chatter stability during the machining process.

Fig. 2b illustrates the forces at play at the interface among the robot, workpiece, and tool. Notably, the force exerted by the proof-mass actuator f_{act} influences the overall support force f_t. However, it is crucial to acknowledge that this support force remains exclusively positive due to the absence of rigid attachment between the robot and the workpiece through the robot-workpiece interface. Additionally, the support force undergoes influence from forces transmitted through the robot's structure itself, necessitating consideration of both the robot's structural dynamics and those of the workpiece in the design of the inertial actuator's control system.

In order to assess the efficacy of this concept in a controlled laboratory environment, previous work has developed a prototype configuration where the robotic manipulator is represented by a simplified structure. The present section validates the findings of that work in a machining environment, using the experimental setup depicted in Fig. 3.

Details concerning the control system design and the control system parameter optimisation are provided in [51] and the relevant system parameters are summarised in Table 1, along with the full parameters of the system.

The transfer function of the actuator can be defined as:

$$\frac{f_{act}(s)}{V_{in}(s)} = 3\frac{s^2}{s^2 + 15.834s + 2785.6} \tag{2}$$

Table 1
Tuning parameters for machining experiments.

Control method	Controller parameters
Direct Velocity Feedback (DVF)	$g_{dvf} = 253$
Virtual Passive Absorber (VPA)	$\mu_c = 0.0061$
Proportional Integrated Derivative (PID)	$g_a = 9.97\times10^{-4}$, $g_v = 256$, $g_p = 2.88\times10^4$
Linear Quadratic Regulator (LQR)	$Q = 8262.4$, $R = 0.028$
H Infinity (H_∞)	$G_{st} = 9.92\times10^5$, $f_1 = 59.12$, $f_2 = 9.95$
μ Synthesis	$G_{st} = 2.2\times10^7$, $f_1 = 4553.84$, $f_2 = 4.29$

Table 2
Structural, machining and actuator parameters.

Preloaded structural parameters		Machining parameters	
Natural frequency	129.3 Hz	Tool diameter	16 mm
Damping ratio	1.34%	Number of teeth	4
Stiffness	1.34×10^7 N m^{-1}	Tool helix angle	45°
Flexible Robot Parameters		Material	Al-7075-T6
Natural frequency	23 Hz, 47 Hz	Cutting stiffness K_r	180×10^6 N m^{-2}
Damping ratio	4.3%, 2.9%	Cutting stiffness K_t	660×10^6 N m^{-2}
Stiffness	0.79×10^6 N m^{-1}, 2×10^6 N m^{-1}	Milling type	Down milling
Actuator Parameters		Radial depth of cut	Half immersion
Natural frequency	8.4 Hz	Feed per tooth	0.05 mm
Damping ratio	0.15		

The experimental setup involved securing the flexible structure onto the CNC table, illustrated in Fig. 3. An Aluminium alloy block (Al 7075-T6, dimensions 100 × 100x300 mm) was used as a workpiece, and the clamping method of the workpiece and the structure of the fixture involve a rigid connection using bolts on a steel box section so as to achieve repeatable dynamic characteristics that could be represented as a single-degree-of-freedom system.

The proof mass actuator was clamped to a steel beam-like structure, which was shaped such that it possessed a low number of dominant modes of vibration and was representative of a serial arm robot. The beam and actuator structure was pushed against the workpiece to ensure positive contact, representing the robot-workpiece interface depicted in Fig. 1.

During milling, measurements of the workpiece and beam accelerations were obtained using an accelerometer (model PCB 353B18). To monitor the spindle speed, a hall-effect sensor was strategically positioned near the tool holder. This sensor detected one revolution of the spindle by capturing changes in voltage caused by the two slots on the tool holder as the spindle rotated. Data acquisition from these experiments was facilitated by a data logger (model NI DAQ USB-4431), enabling comprehensive recording and analysis of experimental parameters and responses.

The milling parameters and tool properties are summarised in Table 2. The cutting operations were conducted on the side opposite to the location of the beam. For the cutting operations, a cutting length of 100 mm was used along with an 8 mm (half) radial immersion for the specified axial depth of cuts. Additionally, the feed direction of the cutting tool was oriented out of the page.

3.1.1. Chatter detection methods

The detection of chatter during machining operations often relies on well-established methods such as once-per-revolution sampling and Fast Fourier Transform (FFT) spectrum analysis, as highlighted in studies like Schmitz et al. [56,57]. These methods capitalise on the periodicity observed in signals during machining, particularly at the tooth passing frequency ($f_{tp} = \frac{N_t N}{60}$, where N is the spindle speed in rpm and N_t is the total number of tool teeth) and their harmonics, especially when non-zero runout occurs. Runout during cutting operations introduces the spindle rotation frequency ($f_s = \frac{N}{60}$) into the FFT spectrum [58]. Frequencies other than these fundamental components in the FFT spectrum often indicate the presence of chatter [59], making FFT analysis a valuable tool for chatter detection.

Another method, once-per-revolution sampling, involves synchronised data collection during cutting operations [57,60]. Davies et al. [60] presented the Poincaré plot, depicting the tool motion in both directions for each revolution. In stable cutting, this plot should demonstrate consistent tool positions across each revolution. However, in the case of chatter, variations in tool position occur from one revolution to another. This disparity is evident in the plot, indicating chatter occurrence. Alternatively, plotting the tool positions in both directions against each other, known as the Poincaré map, can reveal differences. A stable cut exhibits a concentrated cluster of data points, while chatter leads to a dispersed cluster.

In this study, both the once-per-revolution sampling and FFT spectrum methods are employed to detect chatter phenomena. After each cutting operation, these techniques are utilised using acceleration data from the flexible structure. The once-per-revolution sampling method is employed to create Poincaré maps and time-domain plots for each cut, enabling the observation and analysis of tool motion patterns, aiding in the identification of chatter occurrences.

3.2. Machining results

The results obtained from one typical controller – Direct Velocity Feedback control – are first presented in detail, before summarising the performance of the other controllers.

To begin, Fig. 4 provides a visual illustration of the controller performance, by illustrating the surface finish. In the presence of active control (control on), no chatter marks are evident, indicative of a stable cut. However, upon deactivating the control (control off), chatter marks become visible on the cut surface. Fig. 5 presents once-per-revolution samples, Poincaré plot, and FFT spectrum for the corresponding machining conditions. With control, the Poincaré plot shows concentrated data points that are indicative of stable machining. When the controller is switched off, then chatter ensues and this is indicated by the changes in the FFT and the Poincaré plot.

Fig. 6 shows the predicted stability of the system, both with (solid line) and without (dashed line) control. It can be seen that the addition of the DVF controller substantially increases the predicted chatter stability, in line with previously published work [51]. The stability lobe diagram can be predicted using various methods [61,62]. In the present study, stability was predicted using the method developed by Budak and Altintas [4]. While the specifics of this approach are beyond the scope of the current contribution, the theory and methodology are widely reported elsewhere [4,52]. The controlled SLD is obtained using the FRF results after implementing the control method. The present contribution provides rigorous experimental validation of this result through machining trials, as indicated by the markers on Fig. 6. In general, there is reasonably accurate agreement between the experimental data points and the stability predictions. In fact, the results presented in 4 and 5 are one of the unexpected scenarios where the controller was more stable then expected. This could be attributed to structural variations in clamping conditions, leading to small changes in the stability boundaries.

Results at 2800 rpm are presented in Fig. 7 for the scenarios labelled A–D on Fig. 6. Scenarios A (2800 rpm, 0.5 mm depth of cut (doc)) and Point B (2800 rpm, 1.5 mm doc) represent uncontrolled machining. In Scenario A, the Poincaré plot shows concentrated data points that are indicative of stable machining. In Scenario B, an elliptical pattern in the Poincaré plot and the presence of an additional vibration frequency, alongside tooth-pass and run-out frequencies in the FFT spectrum, confirmed an unstable (chatter) cut. These experimental observations align closely with predictions, considering a critical limiting depth of cut of 1.2 mm for the uncontrolled flexible structure.

In the controlled scenario, stability was predicted at Scenario C (2800 rpm, 2.5 mm doc) in accordance with the controlled SLD. However, unexpected stability was observed even at increased depths of cut (Scenario D). Here, the Poincaré plot and the FFT spectrum indicate broadband vibrations in addition to the expected quasi-periodic motion; this was subsequently attributed to the loss-of-contact between the beam-actuator assembly (representing the robotically assisted system) and the workpiece. This result highlights a potential challenge with the implementation of robotic-assisted active vibration control, in that the pre-load applied between the robot and the workpiece must be sufficient to avoid such nonlinear behaviour.

Fig. 8 provides further example data sets under DVF control, for Scenarios E-H on Fig. 6. Scenario E shows an unstable case that matches the predicted stability boundary, and Scenario F is stable as predicted. However, at Scenario G (2100 rpm, 5 mm doc) represents a marginally stable case, where the onset of chatter becomes evident in the FFT spectrum. Finally, Scenario H shows an unstable result, which is particularly important for the present study. Here, the irregularity in the FFT and in the Poincaré section were attributed to actuator saturation effects, with the actuator control signal exceeding the linear range for the proof-mass-actuator and amplifier components.

The experimental outcomes for six control methods are depicted in Fig. 9. Notably, a consistent actuator loss-of-contact issue was observed across all control methods at a spindle speed of 2800 rpm. This observation suggests heightened forced vibrations and structural nonlinearity at this particular spindle speed. Remarkably, the milling experiments imply that the loss-of-contact issue transcends the variation in controller types, highlighting its correlation with the dynamic characteristics of the structure and the specific cutting parameters employed. Therefore, further work may be needed to fully understand the onset of this actuator loss-of-contact phenomenon.

However alongside this, the issue of actuator saturation requires further investigation. To further explore this, additional machining experiments were conducted for DVF control in the region 1700–2250 rpm. It should be noted that the preloaded structural parameters are slightly different than the previous application due to the clamping conditions. The control gains are optimised considering this modification for the saturation predictions. The flexible workpiece, represented by a flexure and an Al 7075-T6 block, exhibits distinct dynamic properties with a natural frequency of 128.1 Hz, a damping ratio of 1.48%, and a stiffness value of 1.13×10^7 N m^{-1}. The results are summarised in Fig. 10. These actuator forces are plotted against the chosen cutting parameters on the SLD, with the saturation islands encircled with red dashed lines. Remarkably, the experimental actuator force data aligns closely with the predicted location of saturation islands, confirming the accuracy of the predicted saturation regions. Here, numerical values indicate the amplitude of the control (command or reference) signal below saturation which is 27 N. It can be seen that the saturation effect appears to exist in isolated islands of the stability diagram and that in some cases the nonlinearity that this introduces means that chatter occurs below the predicted stability boundary. Therefore, this demonstrates that for active vibration control implementations, the issue of actuator saturation must be carefully considered.

4. A new actuator saturation model

This section introduces a new actuator saturation model in the frequency-domain, drawing upon Schmitz's surface location error model [53,63].

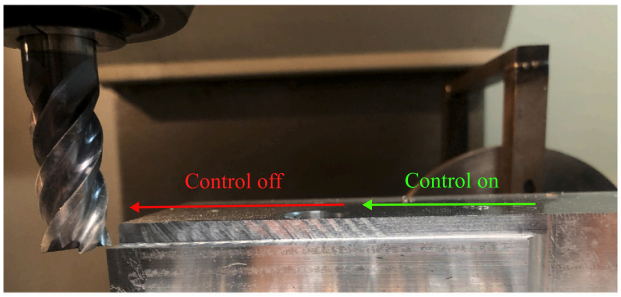

Fig. 4. The chatter marks when the control is on and off with the parameters 2900 rpm, 5 mm doc for DVF controlled structure.

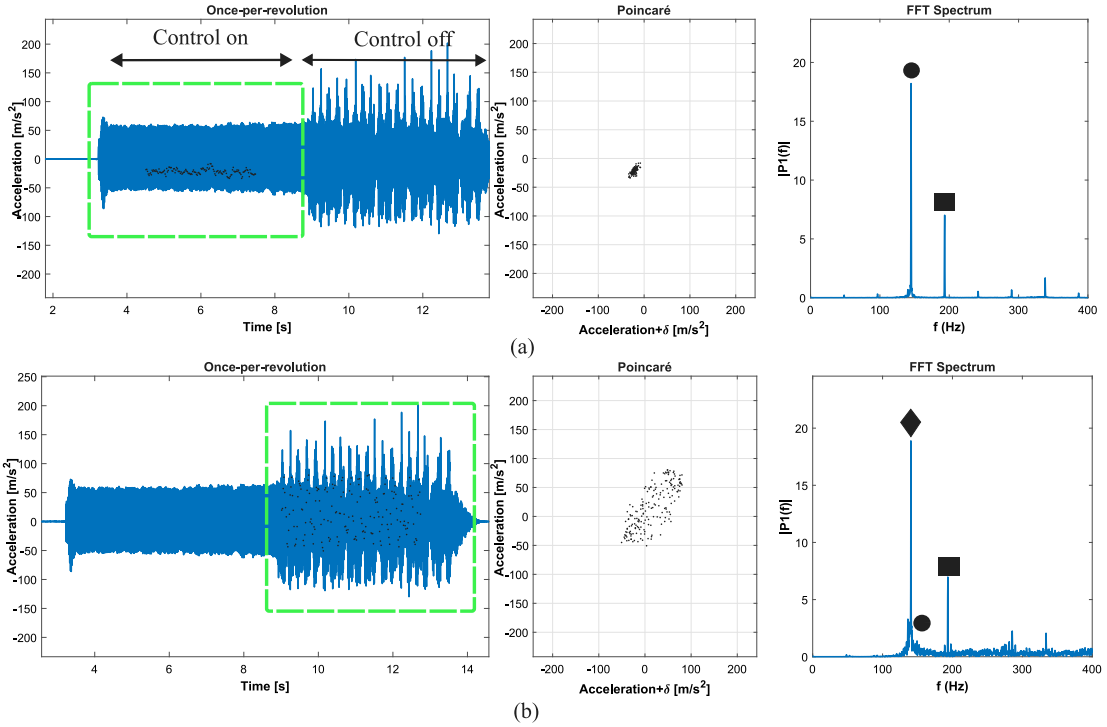

Fig. 5. The chatter marks when the control is on (a) and off (b) with the parameters 2900 rpm, 5 mm doc for DVF controlled structure. Spindle frequency (runout) (●), tooth passing frequency (■), chatter frequency (◆).

4.1. Frequency-domain solution

The methodology introduced by Budak and Altintas [5,7] for SLD prediction was discussed in the previous sections. Their approach involved an analysis of the milling process, expanding the time-varying force coefficients into Fourier series representations. Building upon this framework, this section introduces an actuator force model in the frequency domain, applying Fourier series expansions. The objective of this model is to elucidate the impact and relevance of actuator saturation islands in active vibration control during milling.

To predict these actuator saturation islands using a frequency-domain model, two fundamental assumptions have been considered. Firstly, the actuator force exclusively operates along the y axis while the cutting feed direction remains along the x axis. Secondly, for the scope of stable machining scenarios, any regeneration effect has been omitted. These assumptions serve as the foundation for the subsequent procedural steps:

1. Compute the cutting force in the y direction within the frequency domain, denoted as $F_y(w)$, by employing a Fourier series representation.
2. Determine the displacement $Y(w)$ along the y axis within the frequency domain. Achieve this by multiplying $F_y(w)$ by the FRF of the structure in the y direction.

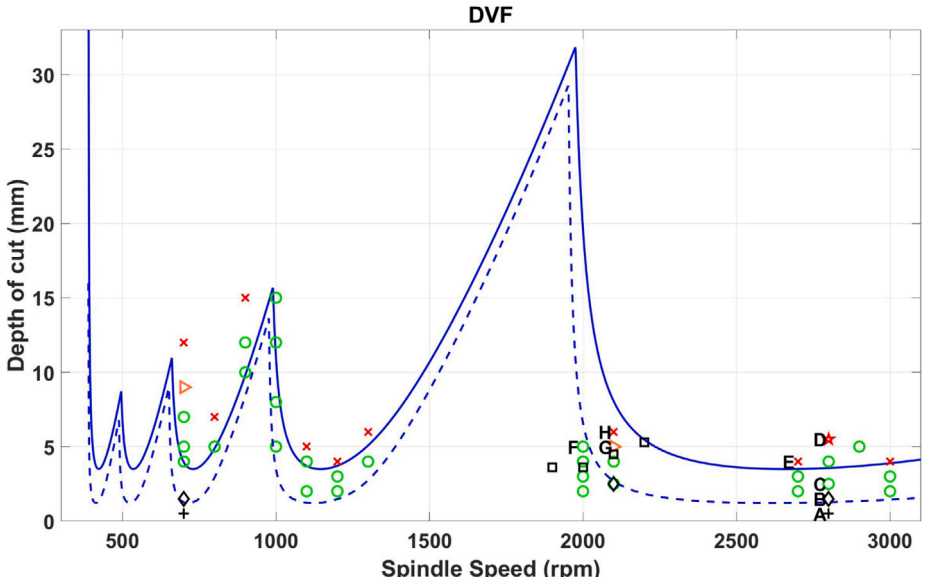

Fig. 6. Stability lobe diagram with experimental results for DVF control method. DVF controlled SLD (——), uncontrolled SLD (- - -), uncontrolled stable cut (+), uncontrolled chatter (◊), controlled stable cut (○), controlled marginal cut (▷), controlled chatter (×), controlled loss-of-contact (★), onset of actuator saturation in time-domain simulation (□).

3. Employ an inverse Fourier transform on $Y(w)$ to transform it back to the time-domain, resulting in the vibration $y(t)$.
4. Derive the voltage value employed by the control method utilising the vibration signal $y(t)$. For example, compute the structure's velocity using $y(t)$, then multiply this velocity by the corresponding gain factor, such as g_{dvf}, to obtain the voltage for DVF control.
5. Calculate the actuator force using the determined voltage value.

4.1.1. *Fourier force model*

The tangential F_t and normal F_n cutting forces are described as:

$$\begin{aligned} F_t(\theta) &= K_t b h(\theta) + K_{te} b \\ F_n(\theta) &= K_n b h(\theta) + K_{ne} b \end{aligned} \tag{3}$$

where K_t, K_{te}, K_n, and K_{ne} are the tangential, tangential edge, normal, and normal edge cutting coefficients, respectively. b and h denote the axial depth of cut and chip thickness.

The cutting force in y direction, $F_y(\theta)$ are described as:

$$\begin{aligned} F_y(\theta) = -b\Bigg[&\frac{-K_t f_t}{2} \sum_{j=1}^{N_t} g(\theta_j)(1-\cos(2\theta_j)) + \frac{K_n f_t}{2} \sum_{j=1}^{N_t} g(\theta_j)(\sin(2\theta_j)) \\ &- K_{te} \sum_{j=1}^{N_t} g(\theta_j)\sin(\theta_j) + K_{ne} \sum_{j=1}^{N_t} g(\theta_j)\cos(\theta_j) \Bigg] \end{aligned} \tag{4}$$

where f_t and N_t are the feed per tooth and total number of teeth, respectively. $g(\theta_j)$ is the switching function which is defined in Eq. (5). The angle of each tooth, j, at any instant in time is $\theta_j = \omega t + \frac{2\pi}{N_t}(j-1)$, (rad), where ω is the spindle rotation frequency (rad/s).

$$g(\theta_j) = \begin{cases} 1, & \theta_s \le \theta_j < \theta_e \\ 0, & \theta_j < \theta_s, \theta_j > \theta_e \end{cases} \tag{5}$$

where θ_s and θ_e are the start and exit tool immersion angles, respectively.

The cutting force in y direction, denoted as F_y, is expressed using the equivalent Fourier series once the Fourier coefficients, a_n and b_n, are computed.

$$F_y(\theta) = \sum_{j=1}^{N_t} \left[a_0 + \sum_{j=1}^{\infty} (a_n \cos(n\theta_j) + b_n \sin(n\theta_j)) \right] \tag{6}$$

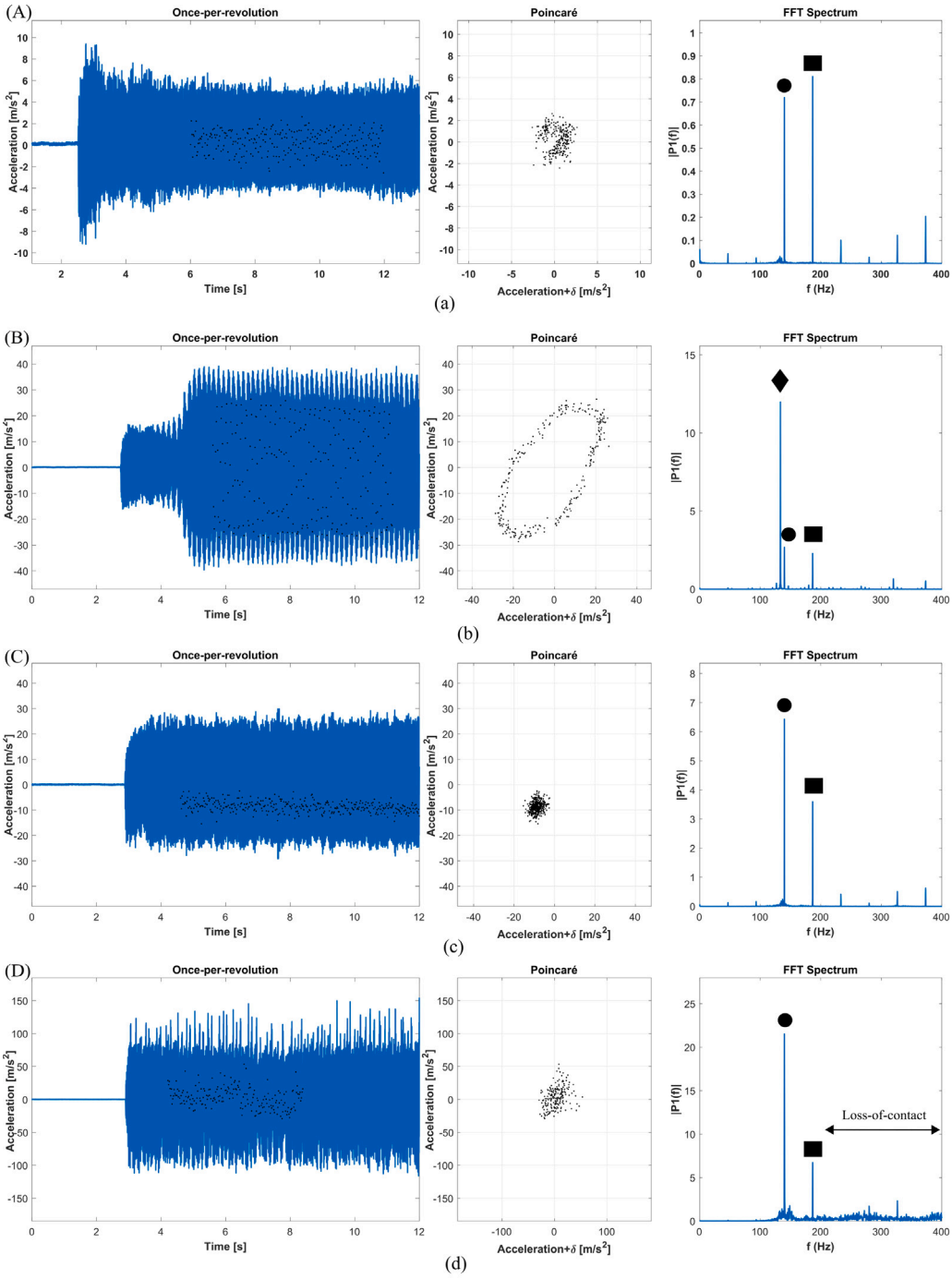

Fig. 7. Once per revolution samples, Poincaré map and the FFT spectrum for (a) stable cut A (2800 rpm, 0.5 mm), (b) chatter cut B (2800 rpm, 1.5 mm), (c) stable cut C (2800 rpm, 2.5 mm), (d) loss-of-contact cut D (2800 rpm, 5.5 mm). Spindle frequency (runout) (●), tooth passing frequency (■), chatter frequency (⧫).

The a_0 term can be defined utilising Eq. (7), where the full revolution of the cutting tool is divided into three parts. θ_1 denotes the entry angle in down milling or exit angle in up milling.

$$a_0 = \frac{1}{2\pi}\int_0^{2\pi} F_y(\theta)\,d\theta = \frac{1}{2\pi}\left[\int_0^{\theta_1} F_y(\theta)\,d\theta + \int_{\theta_1}^{\pi} F_y(\theta)\,d\theta + \int_{\pi}^{2\pi} F_y(\theta)\,d\theta\right] \tag{7}$$

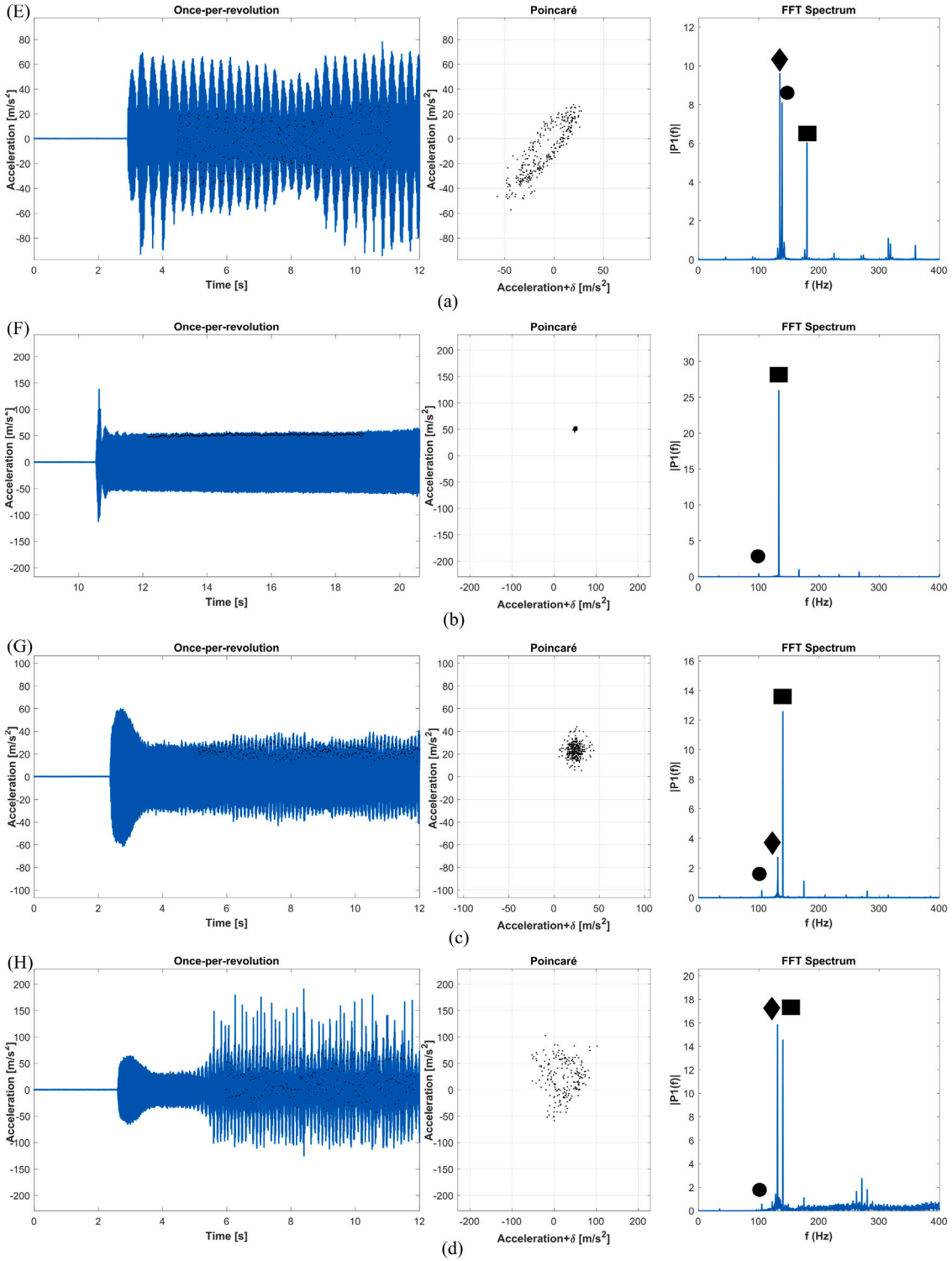

Fig. 8. Once per revolution samples, Poincaré map and the FFT spectrum for (a) chatter cut E (2700 rpm, 4 mm), (b) stable cut F (2000 rpm, 5 mm), (c) marginal cut G (2100 rpm, 5 mm), (d) chatter cut H (2100 rpm, 6 mm). Spindle frequency (runout) (●), tooth passing frequency (■), chatter frequency (⧫).

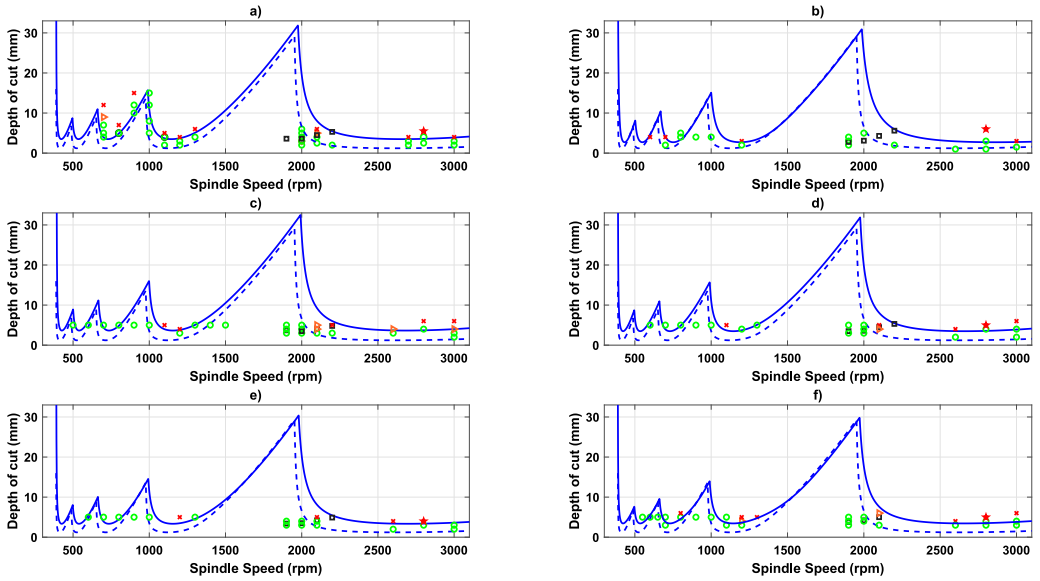

Fig. 9. Stability lobe diagrams with experimental results for (a) DVF control, (b) VPA control, (c) PID control, (d) LQR control, (e) H_∞ control, (f) μ-synthesis control. Controlled SLD (——), uncontrolled SLD (- - -), controlled stable cut (○), controlled marginal cut (▷), controlled chatter (x), controlled loss-of-contact (★), onset of actuator saturation in time-domain simulation (□).

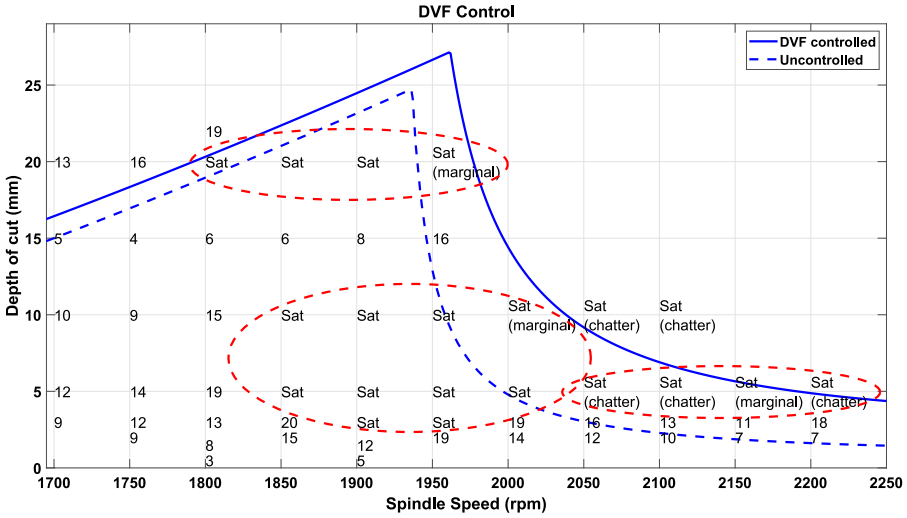

Fig. 10. The predicted saturation islands (encircled with red dashed lines) and experimental actuator forces for DVF controlled system. Controlled SLD (——), uncontrolled SLD (- - -).

If a down milling operation is considered, only the middle integral term is nonzero in Eq. (7) according to the tool engagement, and after the integration process is performed, Eq. (8) is obtained. Otherwise, in up milling, only the first integral term is nonzero, and the integration limits become zero to θ_1 in Eq. (8).

In the case of a down milling operation, considering the tool engagement, only the middle integral term is non-zero in Eq. (7). Upon integration, this leads to the expression given in Eq. (8). Conversely, for up milling, solely the first integral term is non-zero, and the integration limits are adjusted from zero to θ_1 in Eq. (8) (see Fig. 11).

$$a_0 = -\frac{bN_t}{2\pi}\left[-\frac{K_t f_t \theta}{2} + \frac{K_t f_t}{4}\sin(2\theta) - \frac{K_n f_t}{4}\cos(2\theta) + K_{te}\cos(\theta) + K_{ne}\sin(\theta)\right]_{\theta_1}^{\pi} \tag{8}$$

The coefficients a_n and b_n can be defined as:

$$a_n = \frac{1}{\pi}\int_0^{2\pi} F_y(\theta)\cos(n\theta)\,d\theta \tag{9}$$

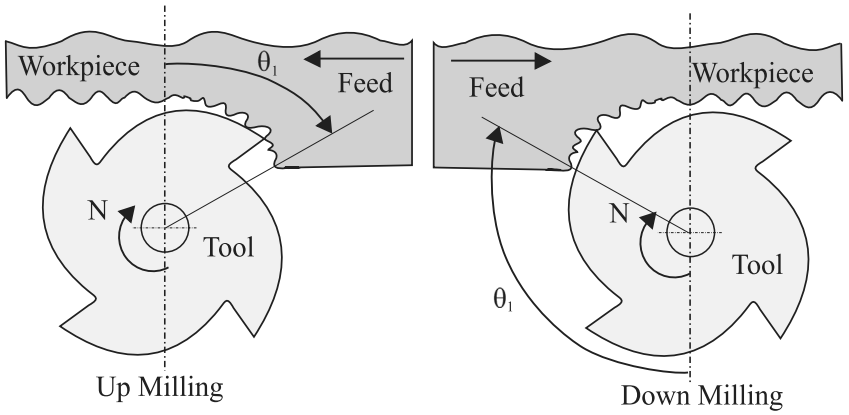

Fig. 11. Angles for the integrals considering the milling type.

$$b_n = \frac{1}{\pi}\int_0^{2\pi} F_y(\theta)\sin(n\theta)\,d\theta \tag{10}$$

The integrals, similar to Eq. (7), can be segmented for the θ and π angles. Following the same recursive patterns of the integration, the equations can be calculated for $n = 3, 4, 5, \ldots$. The Fourier series coefficients $a_1, a_2, a_3, \ldots$ and $b_1, b_2, b_3, \ldots$ are given in Appendix.

To accommodate the helix angle γ in depicting the milling forces, the tool can be divided into A axial segments. Each segment is considered to possess a zero helix angle and is rotated relative to another segment by an angle $\chi = \frac{2db\tan(\gamma)}{d}$, (rad), where db and d are the segment height and the tool diameter, respectively. Subsequently, the Fourier series can be reformulated as follows:

$$F_y(\theta) = \sum_{i=1}^{A}\sum_{j=1}^{N_t}\left[a_0 + \sum_{n=1}^{\infty}(a_n\cos(n\theta_j) + b_n\sin(n\theta_j))\right] \tag{11}$$

where $\theta_j = \omega t + \frac{2\pi}{N_t}(j-1) - \chi(i-1)$. Increased segmentation into a larger number of slices offers a more precise determination of the milling force.

Once the cutting force is calculated, the inverse Fourier transform is applied to $Y(w)$ to obtain the vibration of the structure $y(t)$. In order to implement DVF control, the velocity of the structure is derived from the vibration of the structure $y(t)$. The corresponding voltage value for the controller is then calculated by multiplying this velocity by the gain factor g_{dvf}. Finally, the actuator force is determined using the calculated voltage value, employing the transfer function of the actuator as described in Eq. (2).

4.2. Verification of actuator saturation islands

This subsection aims to experimentally validate the proposed actuator saturation model. In Fig. 12, the predicted actuator saturation is compared to the experimental data that was previously presented in Fig. 10. It can be seen that there is good agreement between the model and experimental data. In particular, a saturation-free region was observed between the predicted saturation islands, confirming the accuracy of the predictive models. Moreover, the second saturation island, projected to occur at higher depths of cut (around 20 mm), was validated by the experimental results, aligning closely with predictions. However, in the region between two SLDs, instances of chatter and marginal cuts with actuator saturation were observed. These arose due to the chosen depth of cuts over the predicted saturation points, exceeding the actuator's capacity to deliver sufficient force. Some disparity emerged between the frequency-domain predictions and experimental results occurred, particularly in the 2050–2200 rpm range. This could be related to actuator loss of contact effects or other nonlinearities.

The comparison between predicted saturation islands in the frequency domain and the experimental outcomes reveals a significant alignment, validating the reliability and accuracy of the frequency-domain predictions.

5. Discussion

Within this section, an analysis is conducted on the actuator saturation model alongside the practical implementation of the concept of robotic-assisted milling.

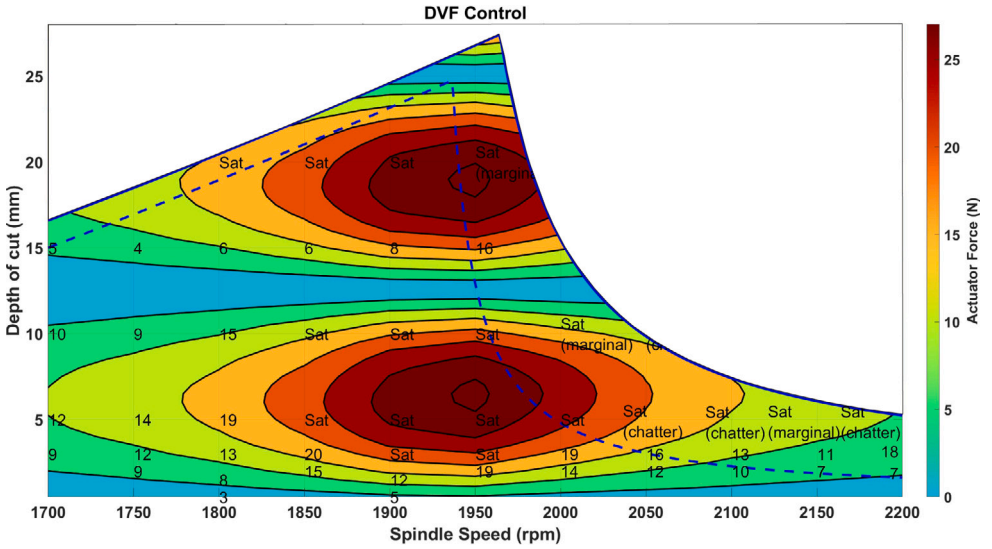

Fig. 12. The predicted saturation islands and experimental actuator forces for DVF controlled system. Controlled SLD (——), uncontrolled SLD (- - -).

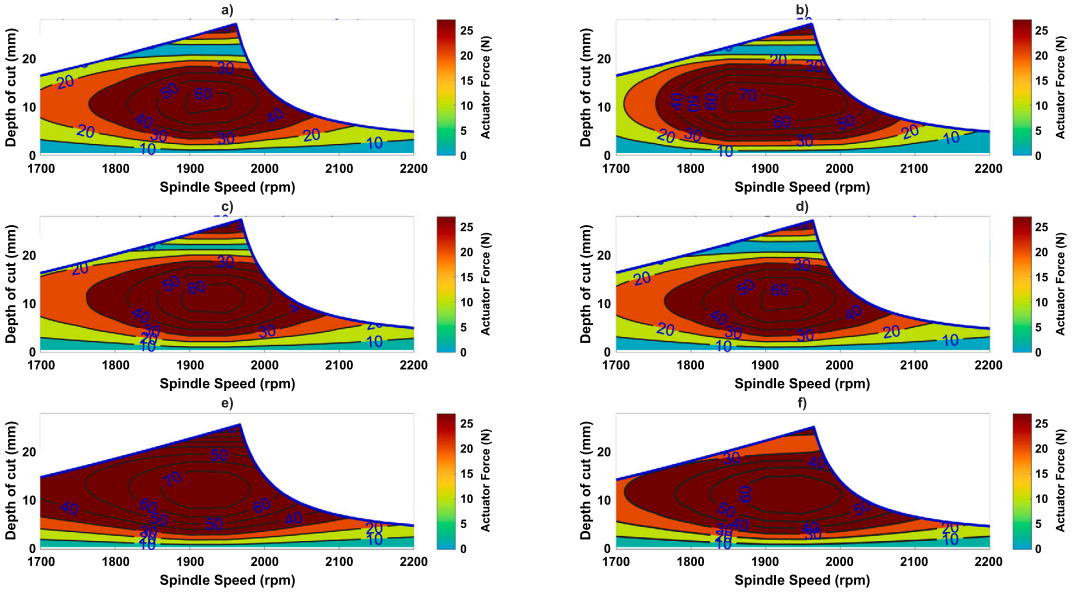

Fig. 13. Actuator saturation islands in frequency-domain for each control method. (a) DVF control, (b) VPA control, (c) PID control, (d) LQR control, (e) H_∞ control, (f) μ-synthesis control.

5.1. Saturation for different control strategies

The detailed procedure in Section 4.1 is employed to identify actuator saturation islands across various controller types. Given the observed actuator saturation occurrence across all control methods near the spindle speed associated with the highest depth of cut, an assessment is conducted within the spindle speed range of 1700 to 2200 rpm. This assessment entails scanning the spindle speed range at 50 rpm intervals, while the axial depth of cut is incremented in intervals of 0.5 mm. This investigation spans from zero to the stability boundary.

The visual representation of saturation islands in the frequency-domain for each control method is presented in Fig. 13. It can be seen that the saturation phenomena is not strongly impacted by the choice of controller. Furthermore, in terms of computational efficiency, the frequency domain method notably outperforms the traditional time domain approaches. Specifically, using 5 and 10 terms of the Fourier force model in the frequency domain method reduces computation time considerably. However, it is worth noting that employing higher terms in the Fourier force model increases the computation time for the frequency domain method.

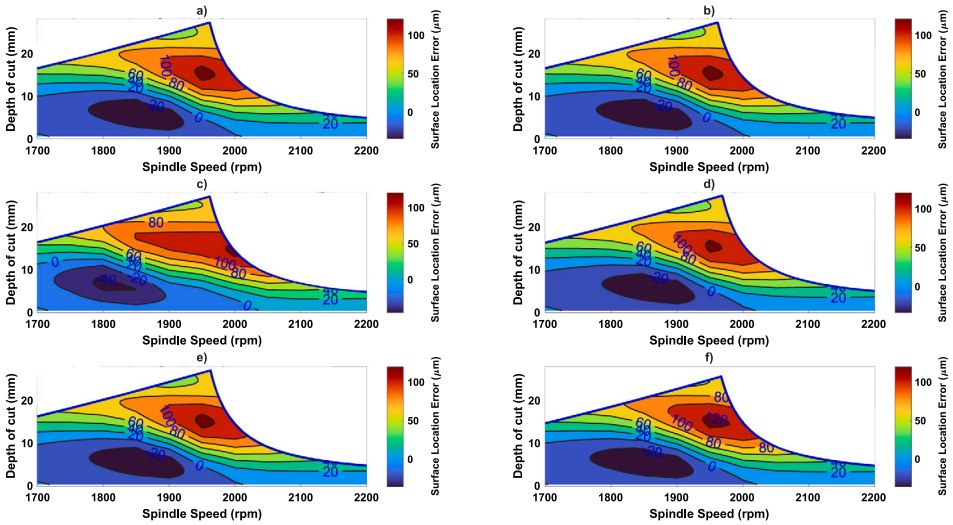

Fig. 14. Surface location errors in freq-domain for each control method. (a) DVF control, (b) VPA control, (c) PID control, (d) LQR control, (e) H_∞ control, (f) μ-synthesis control.

5.2. Relation to surface location error

Fig. 14 displays surface location errors, following the work of [53]. Interestingly, these errors do not mirror the saturation island pattern. They are distinct since surface location errors are determined by tool vibrations at an exact moment, while actuator saturation islands are specifically linked to the vibration difference over time. This comprehension of saturation islands can significantly inform the selection of cutting parameters within the surface location error figures, potentially enhancing material removal rates and operational productivity.

5.3. Influence of helix angle

The influence of the helix angle on the cutting force profile is assessed by examining zero and 45-degree helix angles concerning the DVF control method. The comparison of saturation islands is conducted utilising identical control parameters.

Actuator saturation islands in the frequency-domain are depicted in Figs. 15 for the DVF controlled structure using 45-degree and zero helix angles, respectively. The helix angle significantly influences the number of saturation islands, their respective locations, and actuator forces by affecting the delay in the cutting process. When employing the tool with a 45-degree helix angle, two saturation islands are observed. This is attributed to the helix angle's ability to reduce forced vibrations in the controlled direction, impacting the cutting process delay. In contrast, despite the same number of islands occurring with 30 and 45-degree helix angles, their positions differ.

Conversely, using a tool with a zero helix angle leads to higher forced vibrations in the controlled direction, resulting in a single large saturation island. In this scenario, once saturation begins, it persists until the stability boundary without any intervening saturation-free zones. This observation underlines how varying helix angles influence forced vibrations and subsequent actuator saturation islands during machining.

5.4. Robotic assisted active vibration control milling

The previous discussion has focussed on the broader issue of how actuator saturation can be predicted for active vibration control in milling. However, the scenario presented in the present study has also explored the suitability of this in a robotic-assisted milling scenario. Whilst the proof-of-concept has been experimentally demonstrated in Section 3, some other issues merit further work:

Material removal during cutting might influence the dynamic response of the structure. Consequently, retuning of controller parameters may be needed to ensure optimised controller performance. The incorporation of μ synthesis control, accounting for associated uncertainties, presents a promising area for the robotic-assisted milling concept. In the present study the change in the workpiece dynamics (due to material removal) was negligible.

Potential loss-of-contact issues between the robot and the structure have been observed in the experiments. This requires further investigation, for example by developing analytical predictions and using them to avoid the loss-of-contact occurring. The loss-of-contact could also be addressed by adjusting the robot's position to ensure continuous contact during operation. This can be achieved by maintaining a static preload force higher than the actuator's control force. However, force vibrations or structural nonlinearities could still contribute to loss-of-contact occurrences, potentially preventing the control system's performance.

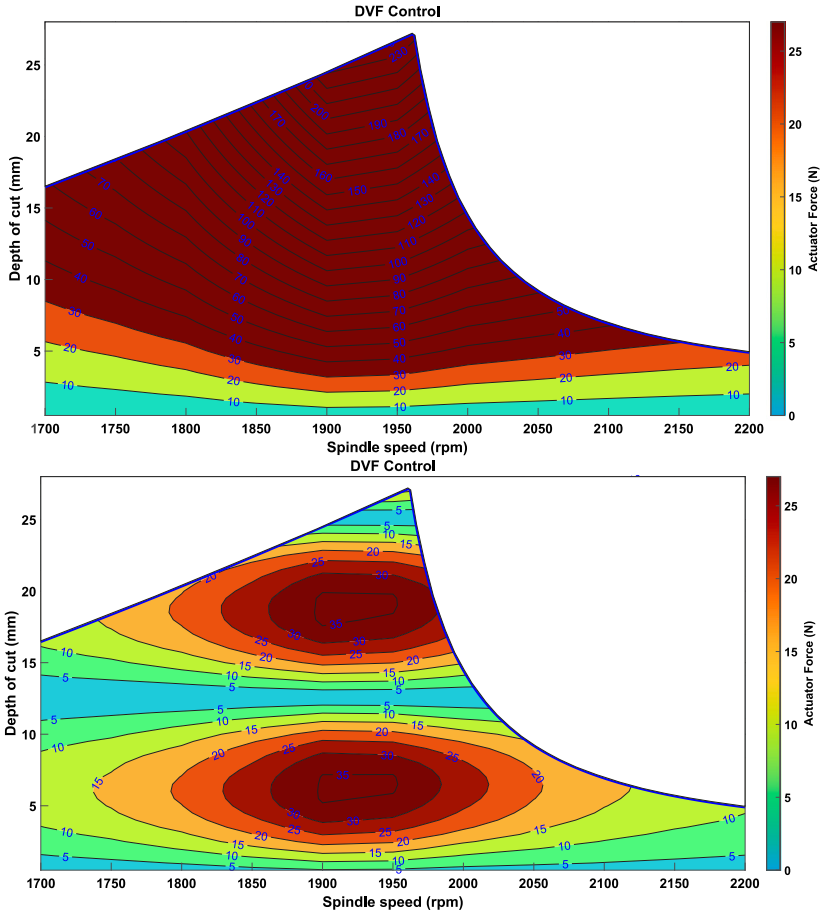

Fig. 15. Actuator saturation islands in frequency-domain, DVF controlled, (a) zero helix angle, (b) 45 helix angle.

Different forms of contact between the robot and the workpiece represent an alternative approach for robotic-assisted milling. While this study utilised rigid metallic contact, employing rolling contact using soft or hard rubber could yield varied system responses due to altered actuator force transmission mechanisms.

Additional modes may emerge during milling, potentially requiring further optimisation of the actuator to achieve optimal performance. Simulation results indicate that the actuator effectively managed multiple vibration modes, including bending and torsion, demonstrating its versatility and reliability when tuned to address these modes.

When chatter occurs during the machining process, selecting appropriate parameters according to the proposed method involves understanding and using saturation islands. By identifying these saturation-free zones, particularly between uncontrolled and controlled stability lobe diagrams (SLDs), optimal cutting parameters can be chosen. This approach helps to:

- Avoid Saturation Zones: Select cutting parameters that fall within regions identified as free from saturation to maintain effective actuator performance.
- Enhance Stability: Choose parameters that align with stable regions of the SLDs, improving overall stability and reducing the likelihood of chatter.
- Increase Productivity: Optimise material removal rates and operational productivity by avoiding conditions that lead to actuator saturation and unstable machining.

6. Conclusion

The conclusions and main contributions from this research that can be drawn are:

- Machining experiments are demonstrated to verify the robotic-assisted milling concept using various control methods (DVF, VPA, PID, LQG, H_∞, and μ synthesis).
- The critical limiting depth of cut (b_{crit}) demonstrates a significant enhancement, increasing by a factor of 2.9 compared to systems without active control and by 4.4 compared to systems lacking robotic-assisted support.

- The practical effectiveness of each controller is assessed via a simplified model and validation experiments, demonstrating strong alignment between predicted stability boundaries and experimental observations.
- A newly proposed predictive model for actuator saturation, based on frequency-domain analysis, is introduced. This model provides insights into how actuator performance can be optimised across different control methods.
- The actuator saturation model with stability lobe diagrams are integrated to identify and avoid saturation-free zones. This integration enhances the accuracy of parameter selection and improves machining stability.
- The predicted saturation islands in the frequency model match with the experimental actuator forces, which demonstrates the model accuracy.
- Additionally, the influence of the helix angle on the location of saturation islands and actuator force is explored, highlighting the impact of cutting tool characteristics on the milling process.

In conclusion, the presented approach demonstrates feasibility in enhancing milling stability via robotic-assisted milling concepts. The experimental verification of a novel actuator saturation model has been conducted. It is shown that practical considerations of actuator saturation, using this model, could offer deeper insights into the performance of active control.

CRediT authorship contribution statement

Muhammet Ozsoy: Writing – original draft, Validation, Software, Methodology, Investigation, Formal analysis, Conceptualization. **Neil D. Sims:** Writing – review & editing, Supervision. **Erdem Ozturk:** Writing – review & editing, Supervision.

Declaration of competing interest

The authors declare that they have no known competing financial interests or personal relationships that could have appeared to influence the work reported in this paper.

Data availability

Data will be made available on request.

Acknowledgements

The first author would like to acknowledge the support from the Turkish Ministry of National Education by providing the scholarship.

Appendix

The Fourier series coefficients

The Fourier coefficients, a_n and b_n, for y direction force series:

$$F_y(\theta) = \sum_{i=1}^{A}\sum_{j=1}^{N_t}\left[a_0 + \sum_{n=1}^{\infty}(a_n\cos(n\theta_j) + b_n\sin(n\theta_j))\right] \tag{12}$$

where $\theta_j = \omega t + \frac{2\pi}{N_t}(j-1) - \chi(i-1)$. The force can be accurately determined by the higher number of slices.

The terms in Eqs. (13) through (18) are determined using Eqs. (9) and (10). Considering the down milling operation, the integration limits become from θ_1 to π, otherwise zero to θ_1.

$$\begin{aligned} a_1 = &-\frac{bN_t}{\pi}\left[K_t f_t\left(-\frac{1}{4}\sin(\theta) + \frac{1}{12}\sin(3\theta)\right) + K_n f_t\left(-\frac{1}{4}\cos(\theta) - \frac{1}{12}\cos(3\theta)\right)\right. \\ &\left. + K_{te}\left(\frac{1}{4}\cos(2\theta)\right) + K_{ne}\left(\frac{1}{2}(\theta) + \frac{1}{4}\sin(2\theta)\right)\right]_{\theta_1}^{\pi} \end{aligned} \tag{13}$$

$$\begin{aligned} a_1 = &-\frac{bN_t}{\pi}\left[K_t f_t\left(\frac{1}{4}(\theta) - \frac{1}{4}\sin(2\theta) + \frac{1}{16}\sin(4\theta)\right) + K_n f_t\left(-\frac{1}{16}\cos(4\theta)\right)\right. \\ &\left. + K_{te}\left(-\frac{1}{2}\cos(\theta) + \frac{1}{6}\cos(3\theta)\right) + K_{ne}\left(\frac{1}{2}\sin(\theta) + \frac{1}{6}\sin(3\theta)\right)\right]_{\theta_1}^{\pi} \end{aligned} \tag{14}$$

$$a_n = -\frac{bN_t}{\pi}\left[K_t f_t\left(-\frac{1}{2n}\sin(n\theta) + \frac{1}{4(n-2)}\sin((n-2)\theta) + \frac{1}{4(n+2)}\sin((n+2)\theta)\right)\right.$$

$$+K_n f_t\left(\frac{1}{4(n-2)}\cos((n-2)\theta)-\frac{1}{4(n+2)}\cos((n+2)\theta)\right)$$
$$+K_{te}\left(-\frac{1}{2(n-1)}\cos((n-1)\theta)+\frac{1}{2(n+1)}\cos((n+1)\theta)\right)$$
$$+K_{ne}\left(-\frac{1}{2(n-1)}\sin((n-1)\theta)+\frac{1}{2(n+1)}\sin((n+1)\theta)\right)\Bigg]_{\theta_1}^{\pi}, n=3,4,.. \tag{15}$$

$$b_1 = -\frac{bN_t}{\pi}\left[K_t f_t\left(\frac{3}{4}\cos(\theta)-\frac{1}{12}\cos(3\theta)\right)+K_n f_t\left(\frac{1}{4}\sin(\theta)-\frac{1}{12}\sin(3\theta)\right)\right.$$
$$\left.+K_{te}\left(-\frac{1}{2}(\theta)+\frac{1}{4}\sin(2\theta)\right)+K_{ne}\left(-\frac{1}{4}\cos(2\theta)\right)\right]_{\theta_1}^{\pi} \tag{16}$$

$$b_2 = -\frac{bN_t}{\pi}\left[K_t f_t\left(\frac{1}{4}\cos(2\theta)-\frac{1}{16}\cos(4\theta)\right)+K_n f_t\left(\frac{1}{4}(\theta)-\frac{1}{16}\sin(4\theta)\right)\right.$$
$$\left.+K_{te}\left(-\frac{1}{2}\sin(\theta)+\frac{1}{6}\sin(3\theta)\right)+K_{ne}\left(-\frac{1}{2}\cos(\theta)-\frac{1}{6}\cos(3\theta)\right)\right]_{\theta_1}^{\pi} \tag{17}$$

$$b_n = -\frac{bN_t}{\pi}\left[K_t f_t\left(\frac{1}{2n}\cos(n\theta)-\frac{1}{4(n-2)}\cos((n-2)\theta)-\frac{1}{4(n+2)}\cos((n+2)\theta)\right)\right.$$
$$+K_n f_t\left(\frac{1}{4(n-2)}\sin((n-2)\theta)-\frac{1}{4(n+2)}\sin((n+2)\theta)\right)$$
$$+K_{te} f_t\left(-\frac{1}{2(n-1)}\sin((n-1)\theta)+\frac{1}{2(n+1)}\sin((n+1)\theta)\right)$$
$$\left.+K_{ne} f_t\left(-\frac{1}{2(n-1)}\cos((n-1)\theta)-\frac{1}{2(n+1)}\cos((n+1)\theta)\right)\right]_{\theta_1}^{\pi}, n=3,4,.. \tag{18}$$

References

[1] G. Quintana, J. Ciurana, Chatter in machining processes: A review, Int. J. Mach. Tools Manuf. 51 (5) (2011) 363–376.
[2] S. Tobias, W. Fishwick, Theory of regenerative machine tool chatter, Engineer 205 (7) (1958) 199–203.
[3] J. Tlusty, M. Polacek, The stability of machine tools against self-excited vibrations in machining, 1963. in: Proceedings of the ASME International.
[4] Y. Altintaş, E. Budak, Analytical prediction of stability lobes in milling, CIRP Ann.-Manuf. Technol. 44 (1) (1995) 357–362.
[5] E. Budak, Y. Altintaş, Analytical prediction of chatter stability in milling—part I: General formulation, J. Dynam. Syst. Measur. Control Trans. ASME 120 (1) (1998) 22–30, [Online]. Available: https://www.scopus.com/inward/record.uri?eid=2-s2.0-13644284085&doi=10.1115%2f1.2801317&partnerID=40&md5=7d8f3f2519406ac409318c25f32eb8ac, Cited by: 616.
[6] Y. Altintas, Analytical prediction of three dimensional chatter stability in milling, JSME Int. J. Ser. C 44 (3) (2001) 717–723.
[7] E. Budak, Y. Altintaş, Analytical prediction of chatter stability in milling—part II: Application of the general formulation to common milling systems, J. Dynam. Syst. Measur. Control Trans. ASME 120 (1) (1998) 31–36, [Online]. Available: https://www.scopus.com/inward/record.uri?eid=2-s2.0-0003021259&doi=10.1115%2f1.2801318&partnerID=40&md5=8b3fdc401bddbded99187a822d6610df, Cited by: 223.
[8] T. Insperger, G. Stépán, Semi-discretization method for delayed systems, Int. J. Numer. Methods Eng. 55 (5) (2002) 503–518.
[9] T. Insperger, G. Stépan, Stability of the milling process, Periodica Polytech. Mech. Eng. 44 (1) (2000) 47–57.
[10] T. Insperger, G. Stépán, Updated semi-discretization method for periodic delay-differential equations with discrete delay, Internat. J. Numer. Methods Engrg. 61 (1) (2004) 117–141.
[11] J. Den Hartog, Mechanical Vibrations, McGraw, Hill, 1934.
[12] N.D. Sims, Vibration absorbers for chatter suppression: A new analytical tuning methodology, J. Sound Vib. 301 (3–5) (2007) 592–607.
[13] Y. Yang, Y. Yang, H.-C. Liu, M. Wan, W.-H. Zhang, A new cutting tool filled with metallic lattice and design method for vibration suppression in milling, Mech. Syst. Signal Process. 212 (2024) 111310.
[14] L. Yuan, S. Sun, Z. Pan, D. Ding, O. Gienke, W. Li, Mode coupling chatter suppression for robotic machining using semi-active magnetorheological elastomers absorber, Mech. Syst. Signal Process. 117 (2019) 221–237.
[15] S. Tobias, Machine Tool Vibration, Blackie, London, 1965.
[16] R. Klein, C. Nachtigal, The application of active control to improve boring bar performance, 1975.
[17] R. Klein, C. Nachtigall, A theoretical basis for the active control of a boring bar operation, 1975.
[18] D. Glaser, C. Nachtigal, Development of a hydraulic chambered, actively controlled boring bar, 1979.
[19] J. Munoa, I. Mancisidor, N. Loix, L. Uriarte, R. Barcena, M. Zatarain, Chatter suppression in ram type travelling column milling machines using a biaxial inertial actuator, CIRP Ann.-Manuf. Technol. 62 (1) (2013) 407–410.
[20] J. Monnin, F. Kuster, K. Wegener, Optimal control for chatter mitigation in milling—Part 1: Modeling and control design, Control Eng. Pract. 24 (2014) 156–166.
[21] J. Monnin, F. Kuster, K. Wegenerr, Optimal control for chatter mitigation in milling—Part 2: Experimental validation, Control Eng. Pract. 24 (2014) 167–175.
[22] Z. Chen, H.-T. Zhang, X. Zhang, H. Ding, Adaptive active chatter control in milling processes, J. Dyn. Syst. Meas. Control 136 (2) (2014) 021007.
[23] D. Li, H. Cao, X. Zhang, X. Chen, R. Yan, Model predictive control based active chatter control in milling process, Mech. Syst. Signal Process. 128 (2019) 266–281.

[24] F. Shi, H. Cao, X. Zhang, X. Chen, A chatter mitigation technique in milling based on H-infinity-ADDPMS and piezoelectric stack actuators, Int. J. Adv. Manuf. Technol. 101 (9) (2019) 2233–2248.
[25] X. Zhang, C. Wang, J. Liu, R. Yan, H. Cao, X. Chen, Robust active control based milling chatter suppression with perturbation model via piezoelectric stack actuators, Mech. Syst. Signal Process. 120 (2019) 808–835.
[26] Y. He, X. Chen, Z. Liu, Y. Chen, Active vibration control of motorized spindle based on mixed h_∞/Kalman filter robust state feedback control, J. Vib. Control 25 (6) (2019) 1279–1293.
[27] Y. Zhang, N.D. Sims, Milling workpiece chatter avoidance using piezoelectric active damping: A feasibility study, Smart Mater. Struct. 14 (6) (2005) N65.
[28] S. Huyanan, N.D. Sims, Vibration control strategies for proof-mass actuators, J. Vib. Control 13 (12) (2007) 1785–1806.
[29] S. Huyanan, An Active Vibration Absorber for Chatter Reduction in Machining (Ph.D. thesis), University of Sheffield, 2007.
[30] X. Beudaert, K. Erkorkmaz, J. Munoa, Portable damping system for chatter suppression on flexible workpieces, CIRP Ann 68 (1) (2019) 423–426.
[31] M. Zaeh, R. Kleinwort, P. Fagerer, Y. Altintas, Automatic tuning of active vibration control systems using inertial actuators, CIRP Ann 66 (1) (2017) 365–368.
[32] R. Kleinwort, J. Herb, P. Kapfinger, M. Sellemond, C. Weiss, M. Buschka, M. Zaeh, Experimental comparison of different automatically tuned control strategies for active vibration control, CIRP J. Manuf. Sci. Technol. 35 (2021) 281–297.
[33] R. Kleinwort, J. Platz, M.F. Zaeh, Adaptive active vibration control for machine tools with highly position-dependent dynamics, Int. J. Autom. Technol. 12 (5) (2018) 631–641.
[34] Y. Altintas, A. Verl, C. Brecher, L. Uriarte, G. Pritschow, Machine tool feed drives, CIRP Annals 60 (2) (2011) 779–796.
[35] K. Erkorkmaz, A. Kamalzadeh, High bandwidth control of ball screw drives, CIRP Annals 55 (1) (2006) 393–398.
[36] H.-C. Möhring, P. Wiederkehr, Intelligent fixtures for high performance machining, Procedia CIRP 46 (2016) 383–390.
[37] C.R. Knospe, Active magnetic bearings for machining applications, Control Eng. Pract. 15 (3) (2007) 307–313.
[38] J. Munoa, X. Beudaert, K. Erkorkmaz, A. Iglesias, A. Barrios, M. Zatarain, Active suppression of structural chatter vibrations using machine drives and accelerometers, CIRP Ann 64 (1) (2015) 385–388.
[39] I. Mancisidor, J. Munoa, R. Barcena, Optimal control laws for chatter suppression using inertial actuator in milling processes, in: 11th International Conference on High Speed Machining, HSM2014, 2014.
[40] M. Law, M. Wabner, U. Frieß, S. Ihlenfeldt, Improving machining performance of in-use machine tools with active damping devices, in: 3rd International Chemnitz Manufacturing Colloquium ICMC, 2014, pp. 393–412.
[41] R. Kleinwort, M. Schweizer, M.F. Zaeh, Comparison of different control strategies for active damping of heavy duty milling operations, Procedia Cirp 46 (2016) 396–399.
[42] M. Ozsoy, N. Sims, E. Ozturk, Improving chatter stability of flexible structure milling in robotic assisted machining, in: ISMA 2022: Proceedings of the International Conference on Noise and Vibration Engineering, International Conference on Noise and Vibration Engineering (ISMA), 2022, pp. 109–120.
[43] N.J. van Dijk, N. van de Wouw, E.J. Doppenberg, H.A. Oosterling, H. Nijmeijer, Robust active chatter control in the high-speed milling process, IEEE Trans. Control Syst. Technol. 20 (4) (2011) 901–917.
[44] M. Ozsoy, H. Dogan, E. Ozturk, D. Wagg, N. Sims, Active chatter suppression through virtual inerter-based passive absorber control, in: Machining Innovations Conference for Aerospace Industry (MIC) 2022, SSRN, 2022.
[45] H. Dogan, N.D. Sims, D.J. Wagg, Design, testing and analysis of a pivoted-bar inerter device used as a vibration absorber, Mech. Syst. Signal Process. 171 (2022) 108893.
[46] H. Dogan., N.D. Sims, D.J. W., Implementation of inerter-based dynamic vibration absorber for chatter suppression, J. Manuf. Sci. Eng. 145 (8) (2023) 084502.
[47] H. Dogan, M. Ozsoy, E. Ozturk, D.J. Wagg, N.D. Sims, Analysis of virtual inerter-based passive absorber for active chatter control, J. Sound Vib. (2024) 118359.
[48] A. Verl, A. Valente, S. Melkote, C. Brecher, E. Ozturk, L.T. Tunc, Robots in machining, CIRP Ann 68 (2) (2019) 799–822.
[49] E. Ozturk, A. Barrios, C. Sun, S. Rajabi, J. Munoa, Robotic assisted milling for increased productivity, CIRP Ann (2018).
[50] M. Ozsoy, N. Sims, E. Ozturk, Investigation of an actively controlled robot arm for vibration suppression in milling, in: EURODYN 2020: Proceedings of the XI International Conference on Structural Dynamics, European Association for Structural Dynamics (EASD), 2020, pp. 4577–4589.
[51] M. Ozsoy, N.D. Sims, E. Ozturk, Robotically assisted active vibration control in milling: A feasibility study, Mech. Syst. Signal Process. 177 (2022) 109152.
[52] Y. Altintas, Manufacturing Automation: Metal Cutting Mechanics, Machine Tool Vibrations, and CNC Design, Cambridge University Press, 2012.
[53] T.L. Schmitz, K.S. Smith, Machining Dynamics, Springer, 2014.
[54] H. Merritt, Theory of self-excited machine-tool chatter: Contribution to machine-tool chatter research-1, J. Eng. Ind. 87 (4) (1965) 447–454.
[55] A. Preumont, Vibration Control of Active Structures, vol. 2, Springer, 1997.
[56] T.L. Schmitz, K. Medicus, B. Dutterer, Exploring once-per-revolution audio signal variance as a chatter indicator, Mach. Sci. Technol. 6 (2) (2002) 215–233.
[57] T.L. Schmitz, Chatter recognition by a statistical evaluation of the synchronously sampled audio signal, J. Sound Vib. 262 (3) (2003) 721–730.
[58] T. Insperger, B.P. Mann, T. Surmann, G. Stépán, On the chatter frequencies of milling processes with runout, Int. J. Mach. Tools Manuf. 48 (10) (2008) 1081–1089.
[59] T. Insperger, G. Stépán, P. Bayly, B. Mann, Multiple chatter frequencies in milling processes, J. Sound Vib. 262 (2) (2003) 333–345.
[60] M.A. Davies, B. Dutterer, J.R. Pratt, A. Schaut, J. Bryan, On the dynamics of high-speed milling with long, slender endmills, CIRP Ann 47 (1) (1998) 55–60.
[61] H. Miao, C. Li, C. Liu, C. Wang, X. Zhang, Nonlinear chatter and reliability analysis of milling Ti-6Al-4V with slender ball-end milling cutter, Mech. Syst. Signal Process. 217 (2024) 111534.
[62] J. Karandikar, K. Saleeby, T. Feldhausen, T. Kurfess, T. Schmitz, S. Smith, Evaluation of automated stability testing in machining through closed-loop control and Bayesian machine learning, Mech. Syst. Signal Process. 181 (2022) 109531.
[63] T.L. Schmitz, B.P. Mann, Closed-form solutions for surface location error in milling, Int. J. Mach. Tools Manuf. 46 (12–13) (2006) 1369–1377.